Time-Reversal: Spatio-temporal focusing and its dependence on channel correlation

Persefoni Kyritsi, and George Papanicolaou

***Abstract*— We study a wireless communications system that applies time reversal to transmit the desired signal, so that it focuses spatially and compresses temporally on the intended receiver. Our theoretical calculations relate the achievable temporal and spatial compression to the channel propagation characteristics and the number of transmit antennas. We illustrate our theoretical results with parameters taken from the IEEE 802.11n channel model. The results verify the intuition that temporal and spatial focusing depend strongly on the delay spread and the angular characteristics of the channel.**

***Index Terms*— Wireless communications, time reversal, delay spread, spatial focusing.**

I. Introduction

TIME reversal (TR) is a method to focus spatially and compress temporally broadband signals through a richly scattering environment [1], [2]. It involves two stages. In the first stage (channel estimation stage), a source emits a short pilot signal. This signal propagates in a richly scattering medium. Its response is recorded by each element of an array that will act as a transmitter in the data transmission stage. The duration of each of these recorded signals is significantly longer than the initial pilot pulse due to multiple scattering. The second stage is the actual data transmission. In this stage, all the elements of the transmitter array send the same data stream, and each one filters the signal to be transmitted through a *time-reversal filter*, *i.e.* a filter that has a form similar to the signal recorded at that particular element during the channel estimation stage, reversed in time (the first portion recorded becomes the last portion transmitted). These transmitted signals focus sharply in space and compress tightly in time at the source location. Moreover, they do so robustly.

Extensive laboratory TR experiments have shown this spatial focus and temporal compression across a broad range of settings in ultrasound experiments (see [3] and references contained therein). In each of these experiments, spatial focusing and temporal compression occur robustly.

Much research activity has been dedicated to using TR for multiple-input/single-output (MISO) underwater communication systems. In fact, several experiments in the ocean have demonstrated MISO-TR communications to be feasible [4]–[8].

Manuscript Draft: October 15, 2007

P. Kyritsi is an Assistant Professor at the Department of Electronic Systems at Aalborg University, Aalborg, Denmark. This work was completed while she was visiting the Department of Mathematics, Stanford University, Stanford, CA (email: persa@es.aau.dk)

G. Papanicolaou is a Professor at the Department of Mathematics, Stanford University, Stanford, CA 94305-2125, USA (email: papanico@math.stanford.edu)

Recently, there has been an effort to apply the principle of TR to electromagnetic waves at radio frequencies. The first experimental demonstration showed that indeed it is possible to achieve temporal compression of wideband signals that are transmitted over the radio channel [9]. A different experiment illustrated the spatial focusing properties of TR for electromagnetic waves using a narrowband system [10]. The post-processing of wideband fixed wireless access channel measurements showed that it is indeed possible to reduce the delay spread of the channel, by using conventional TR or advanced weighting schemes [11], [12]. The same result was shown in a more conventional cellular environment in [13], [14].

Temporal focusing is a desired property because it provides a method to reduce intersymbol interference (ISI). Commonly such an issue is addressed by increasing the receiver complexity using advanced equalization or multi-carrier schemes (*e.g.* OFDM). However, applications such as sensor networks require that the receiver complexity is limited, and the receiver can only perform symbol-by-symbol detection. Such an application would benefit from schemes that lower the ISI.

Spatial focusing on the intended receiver is also a desirable property because it indicates that the communications system has a low probability of intercept (LPI) by another receiver located nearby [15].

Statistical robustness is also a desirable property because it indicates that the spatial and temporal focusing properties are observed consistently over the fading statistics of the channel.

In this paper we study the advantages gained by MISO-TR communication in terms of temporal and spatial focusing and relate them to the channel propagation properties and the system size, under the following assumptions:

- The elements of the transmitting array have perfect Channel State Information (CSI),
- The channel is static, *i.e.* it is the same during both stages of the TR process, as would be consistent with block fading models.

We do not show the statistical robustness of these properties.

For our channel parametrization, we use the IEEE 802.11n channel model that is applicable for systems with bandwidth up to 100 MHz around either 2.5 or 5 GHz. We illustrate the theoretical results and demonstrate that the key parameters are the delay spread (DS) [16] and the angular spread of the channel. Moreover, we show that the implementation of a MISO-TR system results in low signal levels around the intended receiver. For example, our results show that at a distance of one wavelength away from the intended receiver,

the received power is lower than the power on the intended receiver by 10dB.

The remainder of this paper is organized as follows. In Section II we discuss a TR system. In Section III we discuss the channel model that is used for our simulations. In Section IV we show the theoretical results that govern temporal and spatial focusing. Section V illustrates the theoretical results and the effect of the various parameters that affect spatial/ temporal focusing using numerical calculations. The conclusions are summarized in Section VII.

II. System Description

Lower case letters indicate functions in time, whereas upper case letters are used for their frequency domain representation. Bold letters indicate vectors, $\overline{(\cdot)}$ denotes the complex conjugate of the argument $(\cdot)$, and $\otimes$ denotes the convolution operator. $E[\cdot]$ denotes the expectation of the argument $(\cdot)$.

In the following, TX will stand for transmitter while RX for receiver. We look at the baseband representation of the signals and therefore consider them to have spectral content in $[-B/2, B/2]$, where B is the system bandwidth. The actual communication occupies the spectrum $[f_c - B/2, f_c + B/2]$ around the carrier frequency f_c. In the following we denote as $h(t; \mathbf{r}_{TX}, \mathbf{r}_{RX})$ the channel impulse response (CIR) from a transmitter at location $\mathbf{r}_{TX}$ to a receiver at location $\mathbf{r}_{RX}$.

A. Fundamentals of TR Systems

We describe the operation of a downlink communications system with N_{TX} transmit antennas as a two-stage process. The first stage is the *channel estimation*, and the second stage is the *data transmission*.

1) Channel estimation: The first stage is the channel estimation stage, during which each element of the TX array obtains knowledge of the CIR to the intended RX. There are several ways in which channel estimation can be implemented [1]. The accuracy of the channel state information (CSI) at the TX depends on the implementation details, the quantization noise, the additive noise during the process, the repetition rate and the rate of change of the channel. In this paper, we are not concerned with the specifics of the channel estimation and assume that the transmitter has perfect and instantaneous CSI.

[1]Two possible ways in which channel estimation can be implemented are:

- Uplink channel estimation: The intended RX sends a pilot signal, and each element in the transmitting array records the convolution of this pilot signal with the CIR. Based on this, the CIR is estimated. Due to the reciprocity of the channel, this is also the CIR from that transmit array element to the intended RX. This approach can be used in time division duplex (TDD) systems, where the ends of the communication link take turns in sending data.
- Downlink channel estimation: The TXs send training sequences or pilot symbols, and the intended RX estimates the CIR from each transmitting element. It then feeds back this information to the TX array. This approach is more suitable for frequency division duplex (FDD) systems where uplink and downlink communications occupy different parts of the radio spectrum.

2) Data transmission: The second stage is the actual data transmission. The TX uses the CSI it acquired during the channel estimation stage to transmit the signal to the RX. The elements of the transmit array transmit simultaneously the same signal $x(t)$, and each filters it through the time reversed and phase conjugated version of its respective CIR to the intended RX. Let the baseband representation of the signal $x(t)$ to be transmitted be given by

$$x(t) = \sqrt{P} \sum_{k=-\infty}^{\infty} \beta_k \phi(t - kT_s) \tag{1}$$

where P is the transmitted power, and T_s is the symbol time. It denotes the time by which consecutive symbols β_k are separated. It is related to the bandwidth B of the system and the pulse shaping function $\phi(t)$ that is used. The quantity β_k denotes the mapping of the data stream b_k that is destined for the user at $\mathbf{r}_{RX}$ for the modulation scheme used. The constellation points are selected so that $E[|\beta_k|^2] = 1$, in order for the transmit power to be determined by P.

If $g_m(t)$ is the filter at the m-th transmit antenna, then

$$g_m(t) = A \cdot \overline{h(-t; \mathbf{r}_{TX_m}, \mathbf{r}_{RX})} \tag{2}$$

$\mathbf{r}_{TX_m}$ is the location of the m-th transmit antenna. The scaling factor A is determined so that the TR filters do not introduce any signal amplification. It is irrelevant for our analysis and we therefore drop it from our notation.

The received signal at the RX is $y(t)$ and can be written as

$$y(t) = \left(\sum_{m=1}^{N_{TX}} h(t; \mathbf{r}_{TX_m}, \mathbf{r}_{RX}) \otimes \overline{h(-t; \mathbf{r}_{TX_m}, \mathbf{r}_{RX})} \right) \otimes x(t) + n(t), \tag{3}$$

where $n(t)$ is the receiver noise, assumed to be additive white Gaussian noise.

We define the equivalent CIR $h_{eq}(t)$ as

$$h_{\text{eq}}(t) = \sum_{m=1}^{N_{TX}} h(t; \mathbf{r}_{TX_m}, \mathbf{r}_{RX}) \otimes \overline{h(-t; \mathbf{r}_{TX_m}, \mathbf{r}_{RX})}. \tag{4}$$

The equivalent CIR is given as the sum of the autocorrelations of the CIRs to the individual array elements. Therefore it is symmetric around $t = 0$, and achieves its maximum at $t = 0$. This determines the synchronization between TX and RX, as well as the sampling time at the RX.

The inherent assumption in the formulation above is that the channel transfer functions have not changed in the data transmission stage relative to the channel estimation stage. This simplification is valid in slowly varying environments, or when the channel estimation is repeated and the channel state information is updated frequently. The effect of time-varying channels is beyond the scope of this paper.

By the properties of TR in richly scattering media, the signal $y(t)$ is expected to focus spatially at the RX and compress temporally.

B. Temporal focusing

The common measure for the temporal extent of the CIR is the root mean square delay spread (DS), which is defined as the second central moment of the channel power delay profile $pdp(\tau)$:

$$DS = \left(\frac{1}{\int_{-\infty}^{+\infty} pdp(\tau)d\tau} \int_{-\infty}^{+\infty} (\tau - \tau_{mean})^2 \, pdp(\tau)d\tau \right)^{\frac{1}{2}} \tag{5}$$

where

$$pdp(\tau) = E\left[|h(\tau)|^2\right] \tag{6}$$

$$\tau_{mean} = \frac{1}{\int_{-\infty}^{+\infty} pdp(\tau)d\tau} \int_{-\infty}^{+\infty} \tau pdp(\tau)d\tau \tag{7}$$

The power delay profile is calculated as the expected value of the power of the CIR within the local area of the transmitter/ receiver.

In wideband channels, symbol-by-symbol detection is impaired by intersymbol interference (ISI), which is caused by the delayed copies of the signal arriving at the receiver with delays larger than the symbol period. In order to combat ISI, several techniques have been proposed. For example, CDMA systems exploit the delayed channel taps with a rake receiver, and OFDM systems separate the bandwidth into several narrow bands over which there is no ISI. Although ISI is the measure of interest with respect to signal detection, DS is a more commonly used channel related parameter as the system bandwidth increases. Large ISI is commonly associated with high delay spread, and it has been shown that large DS leads to irreducible bit error rate (BER), [17].Therefore in this paper we use the DS as an indication of the temporal compression properties of TR.

C. Spatial Focusing

Let us assume that the system performs TR with a view to communicating with an intended RX that is located at $\mathbf{r}_{RX}$. We are interested in the amount of interference this operation causes at a location $\mathbf{r}' = \mathbf{r}_{RX} + \mathbf{d}$ away from the intended RX.

The reason for this is two-fold:

1) Low interference power at location $\mathbf{r}'$ would mean that it would be possible to simultaneously send data to both locations $\mathbf{r}$ and $\mathbf{r}'$, without impairing each individual communication link. Therefore it impacts the system capacity.
2) The received power away from the intended RX is a measure of the system's probability of intercept. Other information theoretic measures can be used to measure exactly the ability of a system to conceal information from an eavesdropper (e.g. secrecy capacity). However, low power at a distance $\mathbf{d}$ away from the intended RX is an indication that an eavesdropper at that location would not be able to successfully intercept the content of the communication. The problem of an eavesdropper with more sensors than the intended user is an area of ongoing research with respect to information security, but is however beyond the scope of this paper.

We are interested in the spatial distribution of the interference, and therefore consider the equivalent CIR $h_{\text{eq}}(t;\mathbf{r}')$ at location $\mathbf{r}'$:

$$h_{\text{eq}}(t;\mathbf{r}') = \sum_{m=1}^{N_{TX}} h(t;\mathbf{r}_{TX_m},\mathbf{r}') \otimes \overline{h(-t;\mathbf{r}_{TX_m},\mathbf{r}_{RX})} \tag{8}$$

where $h(t;\mathbf{r}_{TX_m},\mathbf{r}')$ indicates the CIR from the m-th TX to $\mathbf{r}'$.

Assuming a perfectly synchronous system, and keeping in mind that the equivalent CIR on the intended RX achieves its maximum at $t = 0$, we concentrate on the value of the interference at that sampling instant, *i.e.* we are interested in:

$$IF(\mathbf{r}') = h_{\text{eq}}(0;\mathbf{r}'). \tag{9}$$

Clearly this is not necessarily the maximum of $h_{\text{eq}}(t;\mathbf{r}')$. It has the advantage though that it lends itself to tractable analytical calculations. For our analysis we will study how the interference decays as the distance from the intended RX grows.

III. Channel model

In the following, we give a brief description of the principles that underlie the IEEE802.11n channel model, so as to smoothly introduce it.

A. Tap delay line model

The CIR of a wideband system can be expressed as a tap delay line model with L taps of the form

$$h(\tau) = \sum_{l=0}^{L-1} h_l \delta(\tau - \tau_l) \tag{10}$$

The l-th tap has complex amplitude h_l and arrives at delay τ_l, and taps that arrive at different delays are assumed to be uncorrelated. For simplicity, we assume that the delays $\tau_l = lT_u$ are the integer multiples of the same time unit T_u for $l = 0, \ldots, L-1$, *i.e.* $\tau_l = lT_u$. The minimum tap spacing relates to the system bandwidth B that the model characterizes. Namely it cannot be above $1/B$. Commonly the tap spacing is taken to be equal to the symbol time, $T_u = T_s$.

The tap amplitudes follow a known power delay profile (pdp)

$$E[|h_l|^2] = pdp(\tau_l) = P_l \tag{11}$$

Using this description, it is possible to have $P_l = 0$ for some values of l.

The statistical distribution of the tap amplitudes depends on the propagation conditions. In this paper we investigate the case where the amplitudes h_l are Rayleigh distributed [18]: let $h_{l,I}$, $h_{l,Q}$ denote the in-phase and quadrature components of h_l respectively. The Rayleigh distribution reflects the case where each tap is the sum of several irresolvable paths, and therefore $h_{l,I}$, $h_{l,Q}$ are independent, identically distributed zero-mean Gaussian random variables with variance $E\left[|\, h_l \,|^2\right]/2 = P_l/2$.

B. Correlation and power azimuth spectrum

We define the random variables

$$\begin{aligned} x &= x_I + j \cdot x_Q = h_l(\mathbf{r}) \\ y &= y_I + j \cdot y_Q = h_l(\mathbf{r}+\mathbf{d}) \end{aligned} \tag{12}$$

x, y denote the complex amplitude of the l-th tap at locations $\mathbf{r}$ and $\mathbf{r}' = \mathbf{r}+\mathbf{d}$ respectively. x_I, y_I denote the in phase components of x, y respectively, and x_Q, y_Q denote the quadrature components of x, y respectively.

For Rayleigh channels, it can easily be shown that the following properties hold for the correlations of x_R, y_I, x_Q, y_Q [19]:

$$R_{x_I y_I} = R_{x_Q y_Q} \tag{13}$$

$$R_{x_I y_Q} = -R_{x_Q y_I} \tag{14}$$

The complex correlation ρ^{IQ} of x, y is given by

$$\rho^{IQ} = R_{x_I y_I} + j R_{x_I y_Q} \tag{15}$$

The cross-correlation between the waves impinging on two antenna elements has been studied in various references, and it has been shown to be a function of the Power Azimuth Spectrum (PAS) and the radiation pattern of the antenna elements. The PAS is often given as a function only of the azimuthal direction ϕ and describes the angular distribution of the received power, *i.e.* $PAS(\phi)$ describes how much power is arriving from the azimuth direction ϕ. Antenna elements will be assumed to be omnidirectional in the following.

Commonly the correlations are calculated for elements that are arranged along the y-axis of the coordinate system. In the general case, the locations of the two elements are separated by $\mathbf{d}$ where

$$\mathbf{d} = d\,(cos\theta\hat{x} + sin\theta\hat{y}) \tag{16}$$

($\hat{x}$, $\hat{y}$ are the unitary vectors along the x and y directions respectively). This means that the two elements are separated by distance d and they have an arbitrary azimuth orientation θ relative to the axis system.

Under these assumptions, the correlations can be calculated according to the following equations [19]:

$$R_{x_I y_I}(\mathbf{d}) = \int_{+\pi}^{-\pi} cos\left(kd\cos(\phi-\theta)\right) PAS\left(\phi\right) d\phi \tag{17}$$

$$R_{x_Q y_I}(\mathbf{d}) = \int_{+\pi}^{-\pi} sin\left(kd\sin(\phi-\theta)\right) PAS\left(\phi\right) d\phi \tag{18}$$

The incidence vector $\mathbf{k}$ is defined for a wave impinging from the azimuth direction ϕ, as

$$\mathbf{k} = \frac{2\pi}{\lambda}\left(cos\phi \cdot \hat{x} + sin\phi \cdot \hat{y}\right) \tag{19}$$

and

In the limiting case of uniform PAS over $[0, 2\pi]$, the correlation is the well-known zero-th order Bessel function of the first kind. In the general case, the PAS is characterized by its shape and clustering characteristics. Several distributions have been used to describe the shape of the angular spread around the mean angle of incidence. Some of the most popular such distributions are the uniform, the truncated Gaussian and the truncated Laplacian ($PAS(\phi) = Ce^{-\sqrt{2}\frac{|\phi|}{\sigma}}, |\phi| \leq \frac{\Delta\phi}{2}$), that have been shown to fit different sets of experimental data. It has also been experimentally observed that radio waves gather in clusters distributed over the azimuth domain [20]. Each cluster has different mean angle of incidence and a different spread around it. Commonly it is assumed that each individual cluster follows the same inner type of distribution. The spread of each cluster around its mean angle of incidence might vary from cluster to cluster.

C. Kronecker model

Let $h_l(\mathbf{r}_{TX_m}, \mathbf{r}_{RX_p})$ denote the complex amplitude of the l-th tap of $h(\tau; \mathbf{r}_{TX_m}, \mathbf{r}_{RX_p})$. Also let $h_l(\mathbf{r}_{TX_n}, \mathbf{r}_{RX_q})$ denote the complex amplitude of the l-th tap of $h(\tau; \mathbf{r}_{TX_n}, \mathbf{r}_{RX_q})$.

The Kronecker property states that the correlation on the transmitting and the receiving sides are separable. Mathematically this is expressed as:

$$\begin{aligned} &\rho^{IQ}(h_l(\mathbf{r}_{TX_m}, \mathbf{r}_{RX_p}), h_l(\mathbf{r}_{TX_n}, \mathbf{r}_{RX_q})) = \\ &\rho_{RX}(\mathbf{r}_{RX_p} - \mathbf{r}_{RX_q}) \cdot \rho_{TX}(\mathbf{r}_{TX_m} - \mathbf{r}_{TX_n}) \end{aligned} \tag{20}$$

The correlation of $h_l(\mathbf{r}_{TX_m}, \mathbf{r}_{RX_p})$ and $h_l(\mathbf{r}_{TX_n}, \mathbf{r}_{RX_q})$ can be factored into two terms: The first term is the receive correlation $\rho_{RX}(\mathbf{r}_{RX_p} - \mathbf{r}_{RX_q})$, which involves only the locations of the receivers p, q. The second term is the transmit correlation $\rho_{TX}(\mathbf{r}_{TX_m} - \mathbf{r}_{TX_n})$ which involves only the locations of the transmitters m, n.

The receive correlations can be intuitively calculated from the PAS around the receiver location (distribution of the angles of arrival (AoA)) as in the previous section. The calculation of the transmit correlations can be done in a similar fashion from the distribution of angles of departure (AoD).

D. The IEEE 802.11n channel model

The IEEE802.11n channel model incorporates the features described in the previous subsections [21]. It consists of a set of 2-dimensional channel models applicable to indoor multiple input- multiple output (MIMO) wireless local area network (WLAN) systems. The models can be used for both the 2.4 GHz and the 5 GHz frequency bands, since experimental data and published results for both bands were used in its development (average, rather than frequency dependent model).

The minimum tap spacing in all the models is $T_u = 10$ ns. Although the IEEE802.11 systems have a bandwidth $B_{802.11n} = 20$ MHz, we can use the models to characterize bandwidths up to $1/T_u = 100$ MHz.

These channel models are an extension of the single input-single output (SISO) WLAN channel models ([22], [23]) to the multiple antenna case, and therefore have known power delay profiles and delay spreads. The original SISO pdp's are consistent with the cluster model developed by Saleh and Valenzuela [24], *i.e.* channel taps arrive clustered in time. The generalization to the MIMO case is based on the assumption that the PAS displays clustering in angle as well as in time, and each temporal cluster is associated with a unique angular cluster. The entries of the MIMO channel transfer matrix are assumed to satisfy the Kronecker property.

The models were developed in a step-wise fashion:

- In each of the three SISO models (A-C) in [22], distinct clusters are first identified. The number of clusters varies from 2 to 6, depending on the model.
- Each channel tap contains power arriving from the direction of one or more clusters, and can therefore be considered as the sum of several independent sub-taps, each corresponding to a different angular cluster. The amount of power of each sub-tap is determined so that the sum of their powers equals the power of the composite tap in the original power delay profile.
- The AoA/ AoD follow the truncated Laplacian distribution. Angular spread (AS), AoA, and AoD values are assigned to each tap and cluster so as to agree with experimentally determined values reported in the literature. The cluster AS was experimentally found to be in the 20^o to 40^o range, and the mean AoA was found to be random with a uniform distribution.
- Given the angular properties of each cluster, the number of subtaps that compose each tap and the power that each one of them contributes, the PAS is defined for each tap.
- The knowledge of the PAS allows as to calculate the correlation of any pair of transmit-receive links, for a given antenna configuration.

At the end of this procedure, 6 channel models were established that differ in delay spread and angular spread and correspond to different types of propagation scenarios. A brief description is shown in Table I. The channel models provide for the case of Ricean fading, by assigning a specific K-factor [2] to the first channel tap in the case of line-of-sight scenarios (assumed to occur up to a break point distance d_{BP}, also specified by the model). The values of the K-factors have been selected so as to match experimental observations and are higher for channels with larger delay spreads.

Model	Delay Spread (ns)	Environment	K-factor (dB)
A	0	Reference	0/-∞
B	15	Residential home/ Office	0/-∞
C	30	Residential home/ Office	0/-∞
D	50	Typical office environment	3/-∞
E	100	Typical large open space	6/-∞
F	150	Large open space	6/-∞

TABLE I
802.11N CHANNEL MODELS

The simulation code was developed based on the software that accompanies the channel model (details can be found in [25]).

E. Models under study

The channel models that we are going to use for our comparison correspond to Models B and C of the IEEE 802.11n specification. In our case, we are interested in local performance around the intended RX. Therefore we are not interested in the absolute power level, and do not incorporate the path-loss model. Moreover, we concentrate on channels that Rayleigh distributed, *i.e.* the taps do not contain a Ricean component (K=0).

Model B corresponds to the environment of a residential building or a small office. The delay spread is 15 ns, and we can clearly distinguish two clusters by visual inspection of the tap delay line. The cluster parameters are summarized in Table II. Fig. 1a shows the tap delay line model for this scenario (not normalized to unit total power).

Model C also corresponds to the environment of a residential building or a small office. Fig. 1b shows the tap delay line model for this scenario (not normalized to unit total power). In contrast to Model B, the delay spread is 30 ns. We can again clearly distinguish two clusters by visual inspection of the tap delay line. The original cluster parameters are summarized in Table III.

Model C has not only longer DS, but also wider angular spread than model B. In order to study the effect of the DS and the angular spread independently, we introduce a modified model C, that has the same pdp as model C, but the same angular parameters as model B. The tap delay line for this model is going to be like the one shown in Fig. 1b, and the angular parameters will be the ones shown in Table II. The comparison of Model B and the modified Model C allows for the illustration of the effect of different DSs. The comparison of Model C and the modified Model C allows for the illustration of the effect of different angular spreads.

Cluster	1	2
Mean AoA	4.3^o	118.4^o
AS (Rx)	14.4^o	25.2^o
Mean AoD	225.1^o	106.5^o
AS (Tx)	14.4^o	25.4^o

TABLE II
ANGULAR PARAMETERS FOR MODEL B

Cluster	1	2
Mean AoA	290.3^o	332.3^o
AS (Rx)	24.6^o	22.4^o
Mean AoD	13.5^o	56.4^o
AS (Tx)	24.7^o	22.5^o

TABLE III
ANGULAR PARAMETERS FOR MODEL C

IV. THEORETICAL RESULTS

In the following we will denote as $\rho_{RX,l}(\mathbf{d})$ the complex correlation of the l-th tap as observed at two locations separated by a distance $\mathbf{d}$. It is a function of the PAS around the receiver of this particular tap, as described in the previous section. Moreover $\rho_{TX,l}(\mathbf{d}_{nm})$ is the transmit correlation of the l-th tap as observed at two transmitters separated by $\mathbf{d}_{nm}$. It is a function of the PAS of the AoD for this particular tap, as described in the previous section.

[2]The K factor is defined as the ratio of the power of the non-fading component over the power of the diffuse signal, the sum of which comprises the Ricean distributed signal.

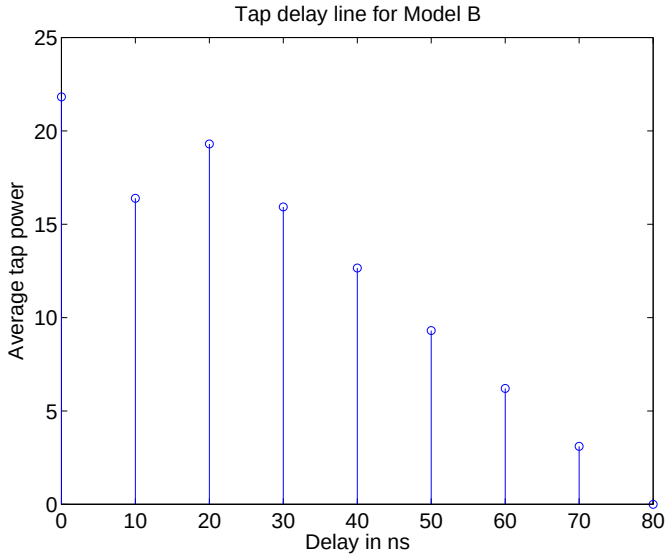

(a) Tap delay line for Model B

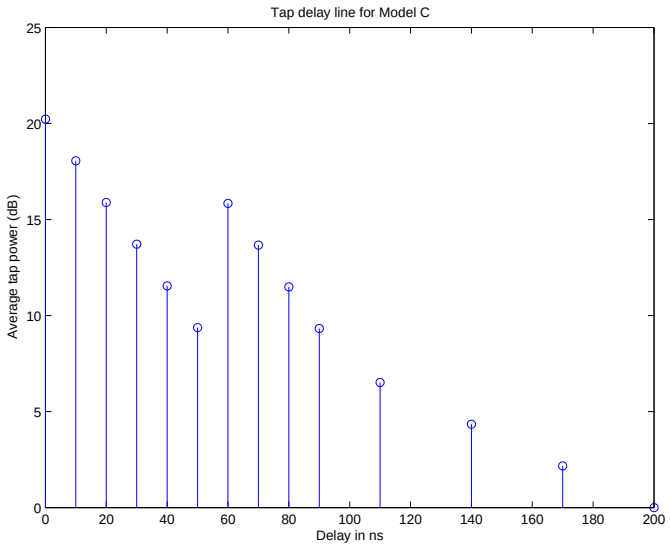

(b) Tap delay line for Model C

Fig. 1. Power delay profiles for (a) Model B, (b) Model C

A. Baseline scenario

Our baseline scenario is single antenna communication over the wireless link without any form of preprocessing at the TX. The CIR from a TX located at $\mathbf{r}_{TX}$ to any receiver location $\mathbf{r}_{RX}$ is given as a tap delay line as in equation (10). The l-th tap has complex amplitude $h_l(\mathbf{r}_{TX}, \mathbf{r}_{RX})$ and arrives at delay τ_l. The tap amplitudes follow a known power delay profile $pdp(\tau_l) = E[|h_l(\mathbf{r}_{TX}, \mathbf{r}_{RX})|^2] = P_l$.

In our baseline case, the DS for the tap delay line model of the channel without TR DS_{noTR} can be calculated from equation (5). We do not expect any special focusing since the assumption of the channel model is that all points around the intended receiver receive the same average power.

B. Single input- Single output (SISO) systems

We first study the case of a single input-single output TR communications system, *i.e.* $N_{TX} = 1$ and the TX performs TR pre-filtering.

After the application of TR at the transmitter, the equivalent CIR can be written as

$$h_{eq}(t; \mathbf{r}_{RX}) = h(t; \mathbf{r}_{TX}, \mathbf{r}_{RX}) \otimes \overline{h(-t); \mathbf{r}_{TX}, \mathbf{r}_{RX}} = \sum_{l=0}^{L-1} \sum_{k=0}^{L-1} h_l(\mathbf{r}_{TX}, \mathbf{r}_{RX}) \cdot \overline{h_k(\mathbf{r}_{TX}, \mathbf{r}_{RX})} \cdot \delta(t - \tau_l + \tau_k) \quad (21)$$

By symmetry

$$h_{eq}(t; \mathbf{r}_{RX}) = \overline{h_{eq}(-t; \mathbf{r}_{RX})} \quad (22)$$

and from (21) and the assumption that $\tau_l = lT_u$ for $m \geq 0$ we have:

$$h_{eq}(mT_u; \mathbf{r}_{RX}) = \sum_{l=m}^{L-1} h_l(\mathbf{r}_{TX}, \mathbf{r}_{RX}) \cdot \overline{h_{l-m}(\mathbf{r}_{TX}, \mathbf{r}_{RX})}. \quad (23)$$

The equivalent CIR after TR has double the temporal extent of the initial CIR. It is an autocorrelation function, that is symmetric around $t = 0$, and achieves its maximum at $t = 0$.

By exploiting the properties of complex Gaussian random variables (see Appendix), we can calculate the power delay profile for the equivalent CIR.

$$E\left[|h_{eq}(0; \mathbf{r}_{RX})|^2\right] = \left(\sum_{l=0}^{L-1} P_l\right)^2 + \sum_{l=0}^{L-1} P_l^2 \quad (24)$$

$$E\left[|h_{eq}(mT_u; \mathbf{r}_{RX})|^2\right] = \sum_{l=|m|}^{L-1} P_l \cdot P_{l-|m|} \quad (25)$$

We observe that

$$\sum_{m=-(L-1)}^{L-1} E\left[|h_{eq}(mT_u; \mathbf{r}_{RX})|^2\right] = 2\left(\sum_{l=0}^{L-1} P_l\right)^2 \quad (26)$$

$$\sum_{m\neq 0} E\left[|h_{eq}(mT_u; \mathbf{r}_{RX})|^2\right] = \left(\sum_{l=0}^{L-1} P_l\right)^2 - \sum_{l=0}^{L-1} P_l^2 \quad (27)$$

Therefore in the limit of large channel length L, the equivalent channel impulse response has as much power in its peak as it does in its tails [3].

Due to the symmetry, we have $\tau_{mean} = 0$. The DS after SISO TR $DS_{TR,N_{TX}=1}$ is

$$DS_{TR,N_{TX}=1} = \left(\frac{1}{\left(\sum_{l=0}^{L-1} P_l\right)^2} \sum_{m=1}^{L-1} m^2 \sum_{l=m}^{L-1} P_l P_{l-m}\right)^{\frac{1}{2}}. \quad (28)$$

Through simple manipulations, it can be shown that

$$DS_{noTR} = DS_{TR,N_{TX}=1} \quad (29)$$

This is a surprising result that indicates that the application of TR from a single transmit antenna does not reduce the perceived DS of the channel. Despite the fact that the equivalent

[3] A similar result was shown in [26] for the case of a pdp that stays constant over all delays. Our result shows that this holds in general for any kind of pdp.

CIR appears to have more energy concentrated around $\tau = 0$, the DS as a 2-norm measure of its temporal extent is unaltered. However, the response is now symmetric, a property that can be exploited to simplify the design of equalizers at the receiver.

We now look at the spatial focusing properties of SISO TR. Using the fact that different taps are uncorrelated and that for complex Gaussian random variables the complex and the power correlation are related (see Appendix), it can be shown that the expected value of the interference power at a location $\mathbf{d}$ away from the intended receiver is given by

$$E\left[|IF(\mathbf{d})|^2\right] = \sum_{l=0}^{L-1} P_l^2 + \sum_{l=0}^{L-1}\sum_{k=0}^{L-1} P_l P_k \rho_{RX,l}(\mathbf{d})\overline{\rho_{RX,k}(\mathbf{d})} \tag{30}$$

The amount of interference depends on the power delay profile and the correlation properties of the taps. As the correlation decreases, we expect this to decrease as well. The expected peak power on the intended receiver ($\mathbf{d} = \mathbf{0}$) is given by

$$E\left[|IF(\mathbf{0})|^2\right] = \sum_{l=0}^{L-1} P_l^2 + \sum_{k=0}^{N_{TX}}\sum_{l=0}^{N_{TX}} P_l P_k \tag{31}$$

C. Multiple input- Single output (MISO) systems

We now study the case of a multiple input-single output (MISO) communications system, *i.e.* when $N_{TX} > 1$. Again the receiver samples the received signal without performing any advanced signal processing, and the transmitter performs TR prefiltering.

After the application of TR at the elements of the Tx array, the equivalent CIR can be written as

$$h_{eq}(t;\mathbf{r}_{RX}) = \sum_{m=1}^{N_{TX}}\sum_{k,l=0}^{L-1} h_l\left(\mathbf{r}_{TX_m},\mathbf{r}_{RX}\right)\overline{h_k\left(\mathbf{r}_{TX_m},\mathbf{r}_{RX}\right)}\delta(t-\tau_l+\tau_k) \tag{32}$$

Again, by symmetry $h_{eq}(t;\mathbf{r}_{RX}) = \overline{h_{eq}(-t;\mathbf{r}_{RX})}$. The equivalent CIR after TR is the sum of autocorrelation functions, and is therefore symmetric around $t = 0$. It also achieves its maximum at $t = 0$. It has double the temporal extent of the initial CIRs, however we expect the autocorrelations to add coherently at $t = 0$, and incoherently off the peak. Therefore we expect the delay spread to be lower than in the baseline case and the SISO TR case.

It can be shown that

$$E\left[|h_{eq}(0;\mathbf{r}_{RX})|^2\right] = N_{TX}^2\left(\sum_{l=0}^{L-1} P_l\right)^2 + \sum_{n=1}^{N_{TX}}\sum_{p=1}^{N_{TX}}\sum_{l=0}^{L-1} P_l^2\left|\rho_{TX,l}(\mathbf{d}_{np})\right|^2 \tag{33}$$

$$E\left[|h_{eq}(mT_u;\mathbf{r}_{RX})|^2\right] = \sum_{n=1}^{N_{TX}}\sum_{p=1}^{N_{TX}}\sum_{l=|m|}^{L-1} P_l P_{l-|m|}\overline{\rho_{TX,l}(\mathbf{d}_{np})}\rho_{TX,l-|m|}(\mathbf{d}_{np}) \tag{34}$$

where $\mathbf{d}_{np} = \mathbf{r}_{TX_n} - \mathbf{r}_{TX_p}$.

By substituting this new power delay profile in equation (5), we can find the perceived DS after TR. If the signals are fully correlated ($\rho_{TX,l}(\mathbf{d}_{n,p}) = 1, \forall\, l,n,p$), then the delay spread stays the same as in the SISO/ baseline case.

If the signals are fully decorrelated ($\rho_{TX,l}(\mathbf{d}_{n,p}) = 0, \forall\, l,n,p$), then

$$DS_{TR,N_{TX}>1} = \frac{1}{\sqrt{N_{TX}}} DS_{noTR} \tag{35}$$

Therefore MISO TR can reduce the DS by a factor of up to $\sqrt{N_{TX}}$ relative to the baseline case.

Let us now concentrate on the amount of achievable spatial focusing in the case of a MISO system. Under the assumption of Rayleigh fading and the separability of the transmit and receive correlations, it can be shown that the expected value of the interference power at a location $\mathbf{d}$ away from the intended RX is given by

$$E[|IF(\mathbf{d})|^2] = \sum_{l=0}^{L-1} P_l^2 \sum_{n=1}^{N_{TX}}\sum_{m=1}^{N_{TX}} \left|\rho_{TX,l}\left(\mathbf{d}_{nm}\right)\right|^2 + N_{TX}^2\left[\sum_{k=0}^{L-1}\sum_{l=0}^{L-1} P_l P_k \rho_{RX,l}(\mathbf{d})\overline{\rho_{RX,k}(\mathbf{d})}\right] \tag{36}$$

The amount of interference depends on the pdp and the correlation properties of the taps, at both the TX and RX sides. As the correlation decreases, we expect this to decrease as well. The expected peak power on the intended RX ($\mathbf{d} = \mathbf{0}$) is given by

$$E[|IF(\mathbf{0})|^2] = \sum_{l=0}^{L-1} P_l^2 \sum_{n=1}^{N_{TX}}\sum_{m=1}^{N_{TX}} \left|\rho_{TX,l}\left(\mathbf{d}_{nm}\right)\right|^2 + N_{TX}^2 \sum_{k=0}^{L-1}\sum_{l=0}^{L-1} P_l P_k \tag{37}$$

In contrast to the SISO case, the power on the intended receiver depends on the transmit correlation as well.

V. Illustration of Theoretical Results

Our purpose is to illustrate graphically the theoretical results of the previous section, and investigate how the various parameters affect the system performance, using the IEEE802.11n channel model.

We are going to compare the following transmission scenarios, namely:

1) Baseline communication, where the TX does not do any pre-processing,
2) SISO TR, where a single TX applies a TR filter and the RX does not perform any equalization, and
3) MISO TR, where N_{TX} TXs apply a TR filters and the RX does not perform any equalization.

The channel models that we are going to investigate are the models presented in Section IIIE, namely: (a) Model B, (b) Model C, and (c) Modified Model C.

The system performance is evaluated in terms of the DS reduction and the achievable spatial focusing.

We want to investigate how these performance measures are affected by:

- Number of transmitters: To illustrate this effect we compare the performance cases of $N_{TX} = 1$ or $N_{TX} = 2$ in an environment described by model B.
- Transmit correlation: To illustrate this effect we compare the performance of a system with two TX antennas ($N_{TX} = 2$), separated by either 0.5λ or 2λ, in an environment that follows the description of model B.
- DS of the original channel model: To illustrate this effect we compare the performance of a single TX system ($N_{TX} = 1$) in two environments described by model B and the modified model C respectively. These have the same angular characteristics but different DS characteristics.
- Angular spread at the receiver: To illustrate this effect we compare the performance of a single TX system ($N_{TX} = 1$) in two environments described by model C and the modified model C respectively. These have the same DS characteristics but different angular characteristics.

A. Delay spread analysis

Table IV shows the delay spread for the three communication scenarios under investigation, and for the three channel models (Model B, Model C, and Modified Model C). The theoretical results have been derived using the definition of the DS (see eq. (5)) and the expected tap powers calculated analytically (see eq. (25) and (33),(34)).

Our first observation is that indeed SISO TR does not reduce the DS of the channel. The larger the TX separation, the lower the transmit correlation, and therefore the greater the reduction in delay spread. Model C has wider angular spread (angle of departure or angle of arrival) than the Modified Model C, and therefore the transmit correlations are lower for the same TX separation. This leads to more significant reduction of the DS by the application of MISO TR.

TABLE IV

RMS DELAY SPREAD COMPARISON

		Theory
Model B	No TR	15.65 ns
	TR ($N_{TX} = 1$)	15.65 ns
	TR ($N_{TX} = 2, sep = 0.5\lambda$)	14.20 ns
	TR ($N_{TX} = 2, sep = 2\lambda$)	12.58 ns
Model C	No TR	33.43 ns
	TR ($N_{TX} = 1$)	33.43 ns
	TR ($N_{TX} = 2, sep = 0.5\lambda$)	27.88 ns
	TR ($N_{TX} = 2, sep = 2\lambda$)	27.30 ns
Mod. Model C	No TR	33.43 ns
	TR ($N_{TX} = 1$)	33.43 ns
	TR ($N_{TX} = 2, sep = 0.5\lambda$)	30.34 ns
	TR ($N_{TX} = 2, sep = 2\lambda$)	26.93 ns

B. Spatial focusing analysis

In the absence of TR, no spatial focusing can be achieved and the average received power is the same at all the locations around the intended RX. Therefore we do not show the result for the baseline scenario.

Fig. 2 shows the expected value of the interference power around the intended RX, assuming that the intended RX is located at the point $(0, 0)$ of our axis system. The results shown have been generated for a channel that follows the description of Model B under the assumption of a single TX antenna and all distances are shown in terms of the wavelength λ. The average received power at any location has been normalized by the average received power on the intended RX, as calculated from the theoretical formulas developed in Section IV. Clearly, the application of TR results in spatial focusing of the power on the intended RX only.

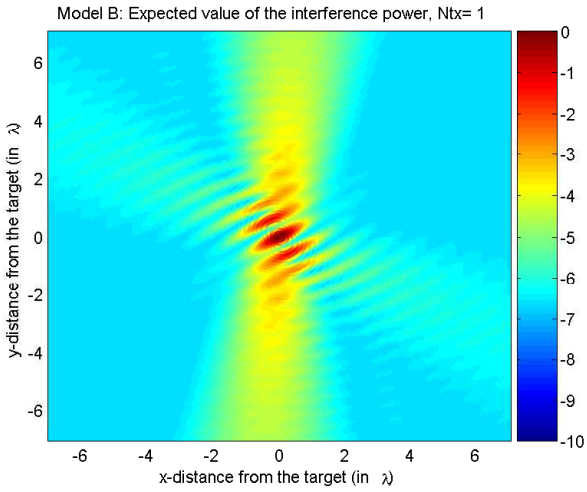

Fig. 2. Spatial focusing in dB for SISO TR

We now look at the effect of transmit correlation. Fig. 3 shows the expected received power around the intended receiver (assumed to be located at $(0, 0)$ of our axis systems) when $N_{TX} = 2$, and the two transmitting antenna elements are separated by either $sep = 0.5\lambda$ or $sep = 2\lambda$ (in the latter situation the transmit correlation is significantly reduced). Again all distances are shown in terms of the wavelength λ.

The comparison of Fig. 3 with Fig. 2 shows that indeed spatial focusing improves with the introduction of more TX elements. It does so more dramatically when the TX elements are less correlated.

The next parameter to investigate is the DS of the channel. For that we compare Model B and the modified Model C that have the same angular characteristics, but different DSs. Fig. 4 shows the expected received power around the intended RX (assumed to be located at $(0, 0)$ of our axis systems) in a channel that follows the description of the modified Model C, assuming that there is a single TX antenna. All distances are shown in terms of the wavelength λ. The comparison of Fig. 4 and Fig. 2 clearly illustrates that increasing the DS of the channel improves the achievable spatial focusing.

Finally, we look at how the angular spread of the channel affects the quality of the spatial focusing. For that we compare Model C and the modified Model C that have the same temporal characteristics, but different angular spreads

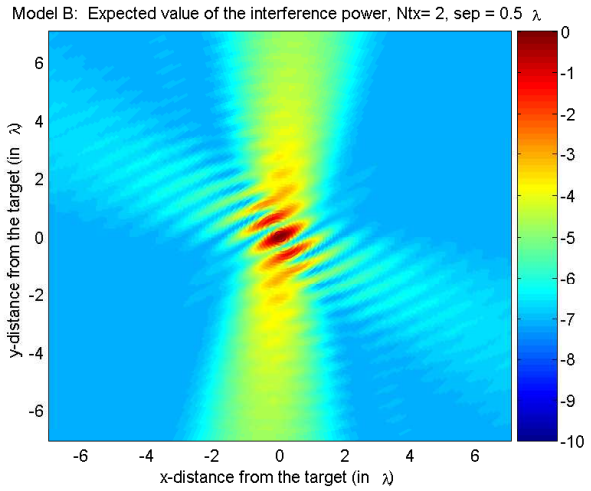

(a) MISO TR ($N_{Tx} = 2, sep = 0.5\lambda$)

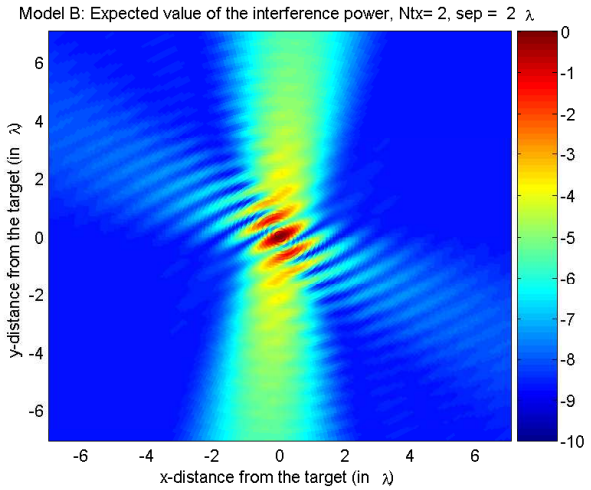

(b) MISO TR ($N_{TX} = 2, sep = 2\lambda$)

Fig. 3. Spatial focusing in dB for MISO TR ($N_{TX} = 2$) (a) $sep = 0.5\lambda$, (a) $sep = 2\lambda$

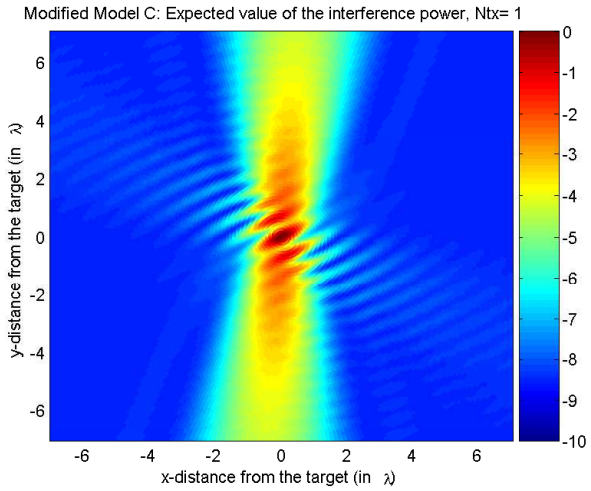

Fig. 4. Spatial focusing in SISO TR for the modified model C

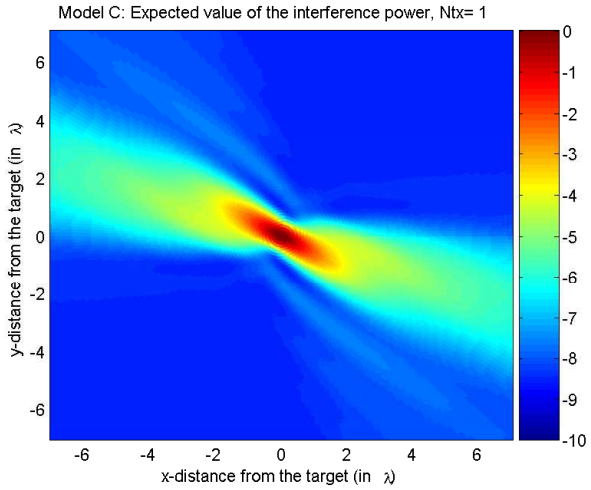

Fig. 5. Spatial focusing in dB for SISO TR with Model C

(Model C has larger angular spread and therefore higher spatial decorrelation). Fig. 5 shows the expected received power around the intended RX (assumed to be located at $(0, 0)$ of our axis systems) in a channel that follows the description of the Model C, assuming that there is a single transmit antenna. All distances are shown in terms of the wavelength λ. The comparison of Fig. 4 and Fig. 5 clearly illustrates that increasing the angular spread of the channel improves the achievable spatial focusing. The two plots decorrelate differently along the x- and y- axes because the clusters in the two models have different mean angles of arrival.

VI. Conclusions

In this paper, we investigated analytically the spatio-temporal focusing potential of the time-reversal technique and how it relates to the channel properties. The theoretical results were illustrated using the channel properties reflected in the IEEE802.11n channel model, that describes typical situations in wireless local area network (WLAN) scenarios.

The application of TR does not reduce the perceived DS of the channel in the SISO situation. In that case, additional signal processing at the RX and/ or the TX is required. The addition of more transmit antennas can reduce the delay spread of the channel. The effectiveness of this technique depends on the channel correlation around the transmitters.

The spatial focusing properties of TR depend on the channel correlation around the intended RX in both the SISO and MISO TR situations.

In summary, increased DS, increased angular spread, more transmit elements and low transmit correlations contribute to increased temporal and spatial focusing. Under sufficient conditions, the received signal is lower by 10dB relative to the intended receiver at distances as short as 1 wavelength away.

Acknowledgment

The work of P. Kyritsi and G. Papanicolaou was supported partially by grants NSF: DMS-0354674-001 and ONR: N00014-02-1-0088.

APPENDIX

The following properties of Gaussian random variables are useful for the derivation of the analytical properties in this paper.

- Higher order moments
  If x is a real, zero-mean, Gaussian random variable with variance σ^2, then

$$\begin{aligned} E[x^2] &= \sigma^2 \\ E[x^4] &= 3\sigma^4 \end{aligned} \tag{38}$$

  If u is a complex, circularly symmetric, zero-mean, Gaussian random variable with variance σ^2, then

$$\begin{aligned} E[|x|^2] &= \sigma^2 \\ E[|x|^4] &= 2\sigma^4 \end{aligned} \tag{39}$$

- Power and complex correlations
  Let x, y be two complex Gaussian random variables. Their complex correlation is defined as

$$\rho^{IQ}(x,y) = \frac{E\left[\overline{x}y\right] - E\left[\overline{x}\right]E\left[y\right]}{\sqrt{\left(E\left[|x|^2\right] - |E\left[x\right]|^2\right)\left(E\left[|y|^2\right] - |E\left[y\right]|^2\right)}} \tag{40}$$

  and their power correlation is defined as

$$\rho^{PWR}(x,y) = \frac{E\left[P_x P_y\right] - E\left[P_x\right]E\left[P_y\right]}{\sqrt{\left(E\left[P_x^2\right] - E\left[P_x\right]^2\right)\left(E\left[P_y^2\right] - E\left[P_y\right]^2\right)}} \tag{41}$$

  where $P_x = |x|^2$, $P_y = |y|^2$.
  The power and complex correlations are related by

$$\rho^{PWR}(x,y) = \left|\rho^{IQ}(x,y)\right|^2 \tag{42}$$

- Product of Gaussians
  Let x_1, x_2, x_3, x_4 be zero-mean, real Gaussian random variables, with covariance matrix C. This means that

$$C_{ij} = E\left[x_i x_j\right] \tag{43}$$

  The expectation of the product $x_1x_2x_3x_4$ is given by

$$E\left[x_1x_2x_3x_4\right] = C_{12}C_{34} + C_{13}C_{24} + C_{14}C_{23} \tag{44}$$

REFERENCES

[1] M. Fink, "Time reversed acoustics," *Physics Today*, March, pp. 33-40, 1997.

[2] M. Fink, "Time-reversed acoustics," *Scientific American*, November, pp. 91-97, 1999.

[3] M. Fink, D. Cassereau, A. Derode, C. Prada, P. Roux, M. Tanter, J-L. Thomas and F. Wu, "Time-reversed acoustics," *Reports on Progress in Physics*, vol. 63, pp. 1933-1995, 2000.

[4] W. A. Kuperman, W. S. Hodgkiss, H. C. Song, T. Akal, C. Ferla, and D. R. Jackson, "Phase conjugation in the ocean: Experimental demonstration of a time reversal mirror," *J. Acoust. Soc. Am.*, vol. 103, pp. 25-40, 1998.

[5] W. S. Hodgkiss, H. C. Song, W. A. Kuperman, T. Akal, C. Ferla and D. R. Jackson, "A long-range and variable focus phase-conjugation experiment in shallow water," *J. Acoust. Soc. Am.*, vol. 105, pp. 1597-1604, 1999.

[6] S. Kim, G. Edelmann, W. S. Hodgkiss, W. A. Kuperman, H. C. Song, and T. Akal, "Spatial resolution of time reversal array in shallow water," *J. Acoust. Soc. Am.*, vol. 110, pp. 820-829, 2001.

[7] G. Edelmann, T. Akal, W. S. Hodgkiss, S. Kim, W. A. Kuperman, H. C. Song, "An initial demonstration underwater acoustic communication using time reversal," *IEEE J. of Oceanic Eng.*, vol. 27, pp. 602-609, 2002.

[8] S. Kim, W. A. Kuperman, W. S. Hodgkiss, H. C. Song, G. Edelmann, and T. Akal, "Robust time reversal focusing in the ocean," *J. Acoust. Soc. Am.*, vol. 114, pp. 145-157, 2003.

[9] G. Lerosey, J. de Rosny, A. Tourin, A. Derode, G. Montaldo, and M. Fink, "Time Reversal of electromagnetic waves," in *Physical Review Letters*, no 92, 2004.

[10] B.E. Henty, D.D. Stancil, "Multipath-enabled super-resolution for rf and microwave communications using phase-conjugate arrays," in *Physical Review Letters*, no 93, December 2004.

[11] P. Kyritsi, G. Papanicolaou, P. Eggers and A. Opera, "MISO time reversal and delay spread compression for FWA channels at 5 GHz," *Antennas and Wireless Propagation Letters* vol. 3, pp. 96-99, 2004.

[12] P. Kyritsi, G. Papanicolaou, P. Eggers, and A. Oprea, "Time reversal techniques for wireless communications," in *Proc. IEEE 60th Vehicular Technology Conference*, Sept. 2004, vol. 1, pp. 47-51.

[13] Hung Tuan Nguyen, J.B. Andersen, G.F. Pedersen, P. Kyritsi, and P.C.F. Eggers, "Time reversal in wireless communications: a measurement-based investigation," in *IEEE Trans. on Wireless Communications*, vol. 5, no 8, pp. 2242-2252, Aug. 2006.

[14] H.T. Nguyen, J.B. Andersen, and G.F. Pedersen, "The potential use of time reversal techniques in multiple element antenna systems," in *IEEE Comm. Letters*, vol. 9, no 1, pp. 40-42, Jan 2005.

[15] A. Kim, P. Kyritsi, P. Blomgren, and G. Papanicolaou, "Low probability of intercept and intersymbol interference in multiple-input/ single-output time reversal communication systems," accepted for publication in *IEEE Journal of Oceanic Engineering*.

[16] C. Oestges, A. D. Kim, G. Papanicolaou, A. J. Paulraj, "Characterization of space-time focusing in time-reversed random fields," in *IEEE Trans. Antennas Propagat.*, vol. 5, pp. 283-293, 2005.

[17] J. Chuang, "The effects of time delay spread on portable radio communications channels with digital modulation," in *IEEE Journal on Selected Areas in Communications*, Vol. 5, no. 5, June 1987, pp. 879 -889.

[18] W.C. Jakes, *Microwave Mobile Communications*, IEEE Press Reprints, New Jersey, 1994.

[19] L. Schumacher, K.I. Pedersen, and P.E. Mogensen, "From antenna spacings to theoretical capacities - guidelines for simulating MIMO systems," in *Proc. 13th IEEE International Symposium on Personal, Indoor and Mobile Radio Communications*, 2002, vol. 2, pp. 587-592.

[20] Chia-Chin Chong, D.I. Laurenson and S. McLaughlin, "Statistical Characterization of the 5.2 GHz wideband directional indoor propagation channels with clustering and correlation properties," in *Proc. IEEE Veh. Technol. Conf.*, vol. 1, Sept. 2002, pp. 629-633.

[21] V. Erceg, L. Schumacher, P. Kyritsi, A. Molisch, D.S. Baum, et al. "TGn channel models," IEEE 802.11-03/940r2, Jan. 2004.

[22] J. Medbo and P. Schramm, "Channel models for HIPERLAN/2," ETSI/BRAN document no. 3ERI085B.

[23] J. Medbo and J-E. Berg, "Measured radiowave propagation characteristics at 5 GHz for typical HIPERLAN/2 scenarios," ETSI/BRAN document no. 3ERI084A.

[24] A.A.M. Saleh and R.A. Valenzuela, "A statistical model for indoor multipath propagation," in *IEEE J. Select. Areas Commun.*, vol. 5, 1987, pp. 128-137.

[25] L. Schumacher, and B. Dijkstra, "Description of a MATLAB implementattion of the indoor MIMO WLAN channel model proposed by the IEEE 802.11 TGn channel model special committee", ftp://ieee:wireless@ftp.802wirelessworld.com/11/03/11-03-0940-04-000n-tgn-channel-models.doc

[26] M. Emami, M. Vu, J. Hansen, A. Paulraj, and G. Papanicolaou, "Matched Filtering with Rate Back-off for Low Complexity Communications in Very Large Delay Spread Channels", in *Proc. Asilomar Conference on Signals, Systems, and Computers*, Nov. 2004.